FINAL TECHNICAL REPORT

Reactivity of Iron-Bearing Minerals and CO_2 Sequestration and Surface Chemistry of Pyrite: An Interdisciplinary Approach

GRANT: DE-FG02-96ER14644

Submitted to the DOE

By

Daniel R. Strongin
Temple University
Philadelphia, PA 19122
Phone: 215-204-7119
Email: dstrongi@temple.edu

December 31, 2014

Abstract

Over the course of the scientific program, two areas of research were pursued: reactions of iron oxides with supercritical CO_2 and sulfide and surface reactivity of pyrite. Both projects were carried out in collaboration with Professor Martin A.A. Schoonen at Stony Brook University. The latter area of interest was to understand the chemistry that results when supercritical CO_2 ($scCO_2$) with H_2S and/or SO_2 in deep saline formations (DFS) contacts iron bearing minerals. Understanding the complexities the sulfur co-injectants introduce is a critical step in developing CO_2 sequestration as a climate-mitigating strategy. The research strategy was to understand macroscopic observations of this chemistry with an atomic/molecular level view using surface analytical techniques. Research showed that the exposure of iron (oxyhdr)oxides (which included ferrihydrite, goethite, and hematite) to $scCO_2$ in the presence of sulfide led to reactions that formed siderite ($FeCO_3$). The results have important implications for the sequestration of CO_2 via carbonation reactions in the Earth's subsurface.

An earlier area of focus in the project was to understand pyrite oxidation in microscopic detail. This understanding was used to understand macroscopic observations of pyrite reactivity. Results obtained from this research led to a better understanding how pyrite reacts in a range of chemical environments. Geochemical and modern surface science techniques were used to understand the chemistry of pyrite in important environmental conditions. The program relied on a strong integration the results of these techniques to provide a fundamental understanding to the macroscopic chemistry exhibited by pyrite in the environment.

Major achievements during these studies included developing an understanding of the surface sites on pyrite that controlled its reactivity under oxidizing conditions. In particular sulfur anion vacancies and/or ferric sites were sites of reactivity. Studies also showed that the adsorption of phospholipid on the surface to selectively suppress the reactivity of these sites could of potential importance for suppressing acid mine drainage in the environment (a problem common to coal-mining sites). Biotic studies showed that microbial activity that promotes the oxidation of pyrite to produce AMD could also be suppressed by the adsorption of phospholipid.

Presentation of Results

The results in this Final report are divided into two parts. The first part of the report concentrates on the interaction of iron oxide bearing phases with supercritical CO_2 and sulfide. The second part is relevant to studies of pyrite reactivity. Included in this latter part are studies that investigated the reactivity of pyrite under both abiotic and biotic conditions with an eye on understanding the microscopic control on reactivity. Publications based on these research projects are listed at the end of the report divided into those relevant to Part I and II.

PART I (Reactivity of Iron-Bearing Minerals and CO2 Sequestration)

Research focused on understanding the transformations of iron oxides and oxyhydroxides to siderite ($FeCO_3$) in the presence of supercritical CO_2 ($scCO_2$) and aqueous sulfide. Techniques used included *in situ* attenuated total reflection Fourier transform infrared spectroscopy (ATR-FTIR), *ex situ* X-ray diffraction (XRD), and aqueous flow through and batch experiments. The initial research in this area focused on the transformations of the iron oxyhydroxide, ferrihydrite and later studies concentrated on pure iron oxide phases present in subsurface environments as well as iron-oxide-bearing sandstones.

A majority of the studies with pure iron-phases focused on hematite with nano-morphologies, denoted by **H1** (~42 nm average particle diameter)and **H2** (average particle diameters of 267 nm) in this report. X-ray diffraction (XRD) data obtained before and after the exposure of **H1** and **H2** particle slurries to $scCO_2$ at 70 °C as a function of the aqueous sulfide concentration are shown in Figure 1. In the figure S1 and S2 refer to sulfide concentrations that are representative of having 2.5 and 5% H_2S in the $scCO_2$. Inspection of the post reaction XRD shows that hematite was partially converted to carbonate and sulfide phases during the exposure to $scCO_2$. All of the experimental conditions resulted in a significant portion of the hematite converting to pyrite and siderite. Analysis of the results showed that the sulfide concentration affects the amount of hematite conversion. For example, the lower sulfide concentration experiment, **S1**, results in ~30% of the iron being converted to siderite and pyrite, and the use of a higher sulfide concentration, **S2**, results in the conversion of about 76% of the iron in the small diameter hematite **(H1)** to iron sulfide and carbonate product. This same trend can be observed for the **H2** sample, but in this case even at the higher sulfide concentration only ~55% of **H2** iron converted in to pyrite and siderite. These experimental observations suggested that the amount of reduction of ferric to ferrous iron and ultimately the amount of hematite conversion to siderite (for a given starting mass of hematite) at the highest sulfide concentrations is greatest for the small diameter particles. We suspect that the increased conversion of **H1S2** relative to **H2S2** is due to the greater initial surface area associated with **H1** (~53 m^2/g) compared to the **H2** sample (~11 m^2/g). The reason why all the hematite does not convert to siderite and pyrite under any of the conditions used in our study is not known, but we speculate that product formation on the hematite particle surface ultimately blocks or prevents the reaction of sulfide with the subsurface region of the hematite particles.

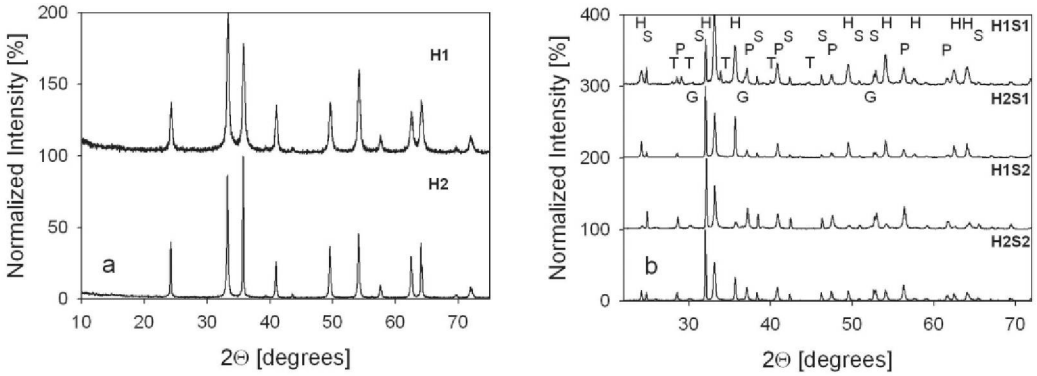

Figure 1: XRD patterns for the a) H1 and H2 starting materials and for b) H1 and H2 after reaction with scCO2 in the presence of 50 mM (S1) or 100 mM (S2) aqueous sulfide (i.e., H1S1, H2S1, H1S2, and H2S2). Labels on the XRD pattern refer to hematite (H), siderite (S), pyrite (P), trona (T), and greigite (G).1

It is important to note that in all cases the reaction with hematite led to equimolar amounts of siderite and pyrite. This particular experimental observation suggests that the following reactions dictate the outcome of the experiment:

$$2Fe^{3+} + 2S^{2-}(aq) \rightarrow FeS_2(pyrite) + Fe^{2+}(aq) \quad (1)$$

$$Fe^{2+}(aq) + CO_3^{2-}(aq) \rightarrow FeCO_3(siderite) \quad (2)$$

In this reaction scheme, every mole of pyrite produced from ferric iron and sulfide produces one mole of ferrous iron that reacts with carbonate to form siderite (reactions **1** and **2**).

In an attempt to gain further insight, ATR-FTIR was carried out to monitor the reaction between $scCO_2$, sulfide, and hematite in situ. Figure 2 exhibits in situ ATR-FTIR data for **H1** during exposure to $scCO_2$ at 70 °C with and without sulfide **S2** as a function of reaction time. Upon pressurizing the system with $scCO_2$, an intense and sharp CO_2 absorbance appears at 2340 cm^{-1} (asymmetric stretch, see inset). Within 5 minutes a peak attributed to bicarbonate grows in at ~1360 cm^{-1}. Siderite formation is observed within 5 minutes of heating to 70 °C as evidenced at least in part by the growth of the broad peak that is initially centered at ~1400 cm^{-1}. Other distinguishing peaks for siderite grow in at ~865 (ν_2) and ~740 (ν_4) cm^{-1} and they are attributed to the carbonate out of plane and in plane bends, respectively. Over the course of 4 h these peaks continue to increase, although at a diminishing rate. After 4 h, there is little change in the intensity of the

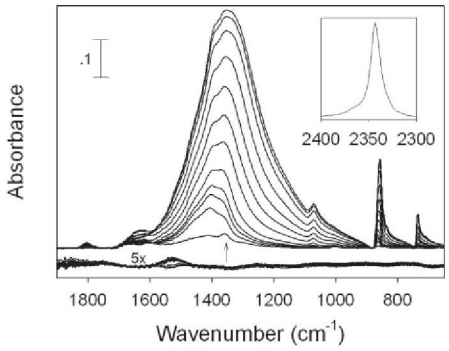

Figure 2: In situ ATR-FTIR data associated with the transformation of nano hematite to siderite in the presence of supercritical carbon dioxide and sulfide. All spectra were taken at 70°C under 82 bar CO_2 and are offset for clarity. Siderite formation becomes noticeable from these data after 1 h of reaction time. Pyrite is another reaction product.2

siderite peaks. The **H1S2** spectrum results in a stronger absorbance than **H1S1** (not shown) which is consistent with the XRD results that show that this sample leads to a higher conversion of hematite to siderite. These results taken as a whole show that the transformation of stable oxides such as hematite can be converted to stable carbonates. These results suggests that a portion of the $scCO_2$ injectate may become mineralized during the future subsurface storage of $scCO_2$.

The effort in the Strongin group was complemented by aqueous experimental work in Martin Schoonen's group at Stony Brook University. Flow-through experiments and batch experiments (70°C) were conducted to determine the reactivity of crushed, iron-bearing sandstones to $scCO_2$ containing H_2S and/or H_2SO_3. The flow-through experiments are conducted in a newly developed system that allows advection of $scCO_2$ over a column of crushed sandstone. The system has the option to mix an aqueous H_2S or H_2SO_3 in the $scCO_2$ stream before it enters the column. The conditions in these flow-through experiments simulate the conditions near the injection point. Batch experiments in

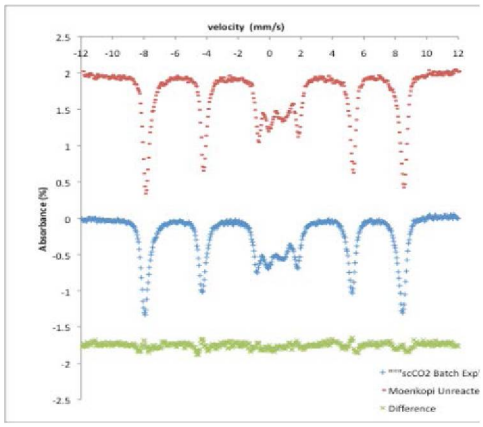

Figure 3: Mössbauer spectra for red sandstone reacted with $scCO_2$. Unreacted sandstone (top), reacted (middle), difference (bottom)3.red sandstone reacted with $scCO_2$. Unreacted sandstone (top), reacted (middle), difference (bottom)3.

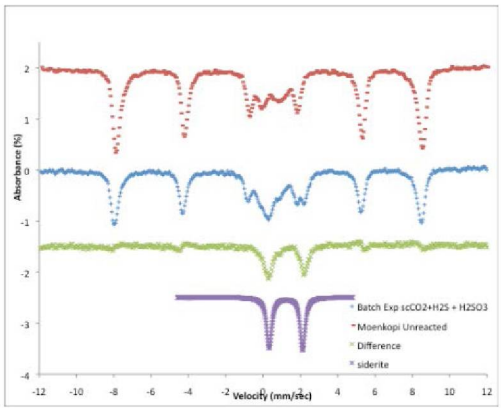

Figure 4: Mossbauer spectrum for red sandstone reacted with $scCO_2$ and aqueous sulfide solution. Unreacted (top), reacted (second down), difference (third down), siderite (bottom).

which $scCO_2$ coexist with an aqueous phase complement the flow-through experiments. These experiments were conducted by adding dry ice to a small volume of rock slurry. At the conclusion of the experiments the materials are recovered and examined with XRD, TGA, and Mössbauer Spectroscopy. Mössbauer spectroscopy was particularly useful because it allow one to determine the changes in iron mineralogy, despite the fact that the iron content of the sandstone is less than 1-2 wt%. Consistent with the result obtained with pure iron (hydr)oxide phases, the sandstone show only a change in the iron mineralogy when sulfide is present. Figure 3 shows Mössbauer spectra for an unreacted red sandstone, the same sandstone exposed to water and $scCO_2$, and a difference spectrum. Figure 4 shows the same sandstone but now reacted with $scCO_2$ and an aqueous sulfide solution. The difference spectrum shown in Figure 4 shows a gain in absorbance consistent with the formation of siderite.

We also extended our studies to more closely match those conditions that may be used in future CO_2 sequestration technology. Specifically, we have recently conducted preliminary investigations concerned with the reaction of aqueous suspensions of hematite with $scCO_2$ with 0.5-2% H_2S. These experiments used gaseous H_2S (rather than aqueous sulfide as a proxy) to take us closer to actual CO_2 sequestration conditions. The results (see Figure 5) showed that as the pressure of H_2S is increased there is a more significant conversion of the ferric bearing mineral (i.e., hematite) to pyrite and siderite.

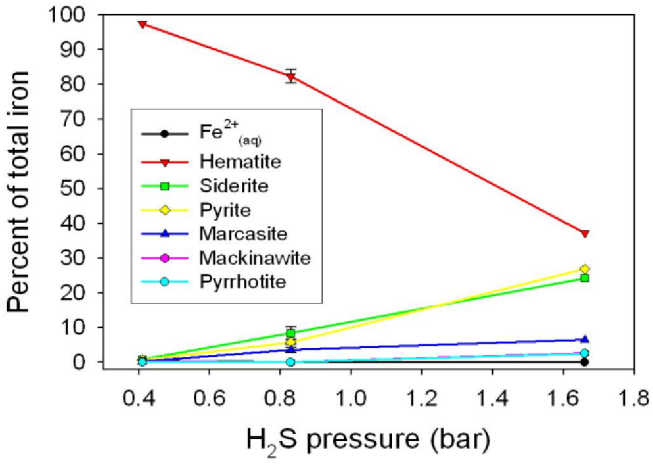

Figure 5: Product distribution as a function of H_2S pressure in the scCO2 injectate (total pressure 85 bar). More siderite is formed as the concentration of H_2S in the $scCO_2$ increases (at least up to 2%).

PART II (Surface Chemistry of Pyrite)

Surface reactivity of Pyrite in the abiotic environment

Research fell into three areas: (A) micro- and macroscopic studies of the adsorption of bilayer forming lipids on pyrite; (B) attenuated total reflection Fourier transform infra red spectroscopic studies of the pyrite oxidation mechanism; and (C) studies designed to determine the nature and reactivity of defects on the pyrite surface.

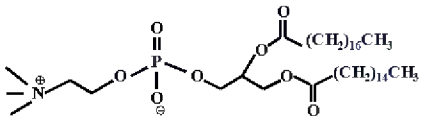

Phosphatidylcholine (egg PC)

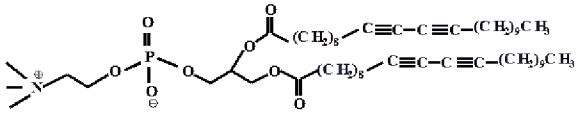

1,2-bis(10,12-tricosadiynoyl)-*sn*-Glycero-3-Phosphocholine (23:2 Diyne PC)

Figure 6: Schematics of two lipids investigated on pyrite with regard to oxidation suppression.

Lipid adsorption on Pyrite

Research addressed the solution of a significant environmental problem referred to as Acid mine drainage (AMD), resulting from the oxidation of metal-sulfides, primarily pyrite. This environmental impact includes acidification of rivers and streams as well as leaching of toxic metals from the metal-sulfide material. Prior research in our laboratory showed that the adsorption of two-tail lipids, such as L-α-Phosphatidylcholine, Hydrogenated

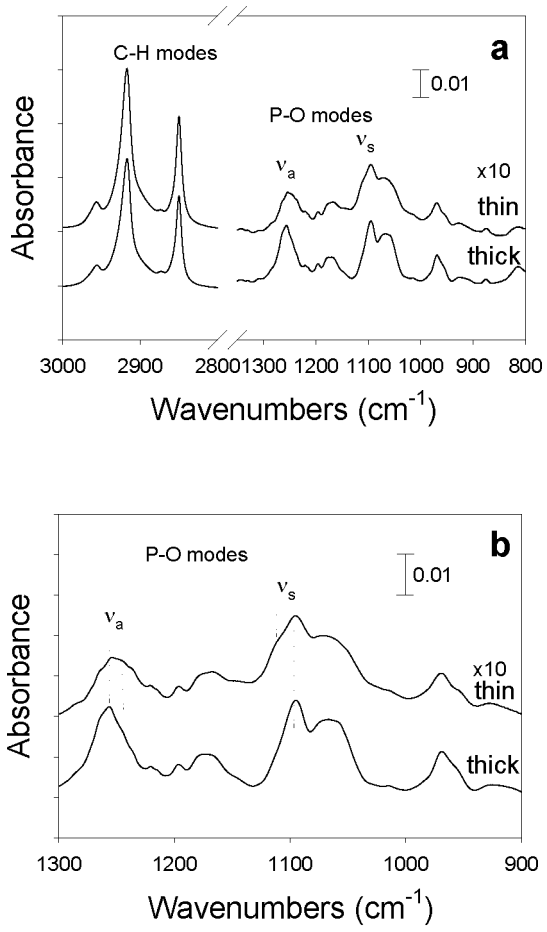

Figure 7: ATR-FTIR of egg PC on pyrite. (A) wide range and (B) narrow scan in phosphate vibration region.

(Egg, Chicken) lipid and 1,2-bis(10,12-tricosadiynoyl)-*sn*-Glycero-3-Phosphocholine on pyrite resulted in a marked decrease in oxidation rate. Research then investigated the microscopic aspects of the bonding of phosphocholine lipids to the pyrite surface.

ATR-FTIR of the lipid pyrite interface

Figure 6 exhibits schematic structures of two phosphocholine lipids that were investigated. Figure 7 exhibits ATR-FTIR data for egg PC (top schematic in Figure 6) on pyrite powder. Part A of Figure 7 exhibits both the C-H and P-O stretching regions of this particular lipid. Figure 2b exhibits a narrower window that emphasizes the symmetric and antisymmetric P-O stretching region. These data show that a thin layer of lipid (bilayer) exhibits resolvable features that are associated with the bonding of the phosphate group of the lipid with the pyrite surface.

Figure 8 exhibits an atomic force microscope (AFM) image of the lipid covered pyrite surface. The interior square of the image is where the AFM tip was used to remove lipid, allowing the lipid height to be measured relative to the pyrite surface. The height measured was approximated 50 Å, twice the length of a single egg PC molecule. This results confirms that the lipid forms a protective *bilayer* coating on the pyrite surface.

Pyrite oxidation inhibition by a cross-linked lipid coating

Additional research addressed the effect of a diacetylene-containing phospholipid on the oxidation rate of pyrite, FeS_2. Earlier work reported by our research group showed that the adsorption of 1,2-bis(10,12-tricosadiynoyl)-sn-Glycero-3-Phosphocholine on pyrite suppressed the extent of its oxidation by about 75% over a specific time period. Results obtained showed that the pre-exposure to UV radiation of this lipid after sorption onto pyrite results in a 90% suppression (Figure 9). Attenuated total reflection (ATR) Fourier Transform Infra-red Spectroscopy (FTIR) suggested that the UV irradiation of the lipid does not result in degradation of the adsorbed layer. It is believed that the UV exposure results in the cross-linking and polymerization of the adsorbed phospholipid into a relatively impermeable barrier that separates the pyrite from the aqueous phase. The results of this study might have implications for the protection of pyrite from oxidation in the environment.

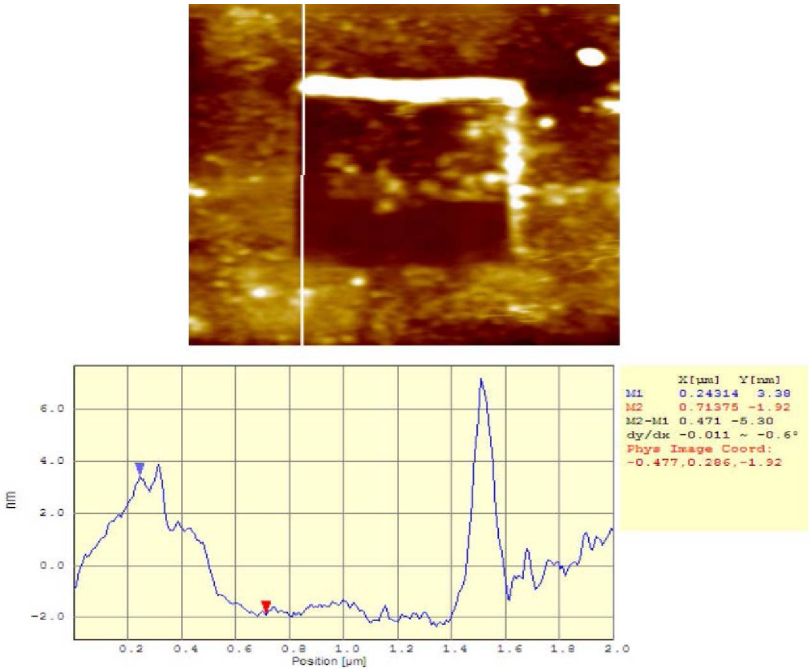

Figure 8: Top: AFM image of egg PC on the pyrite surface. Bottom: cross sectional height information for white line in top.

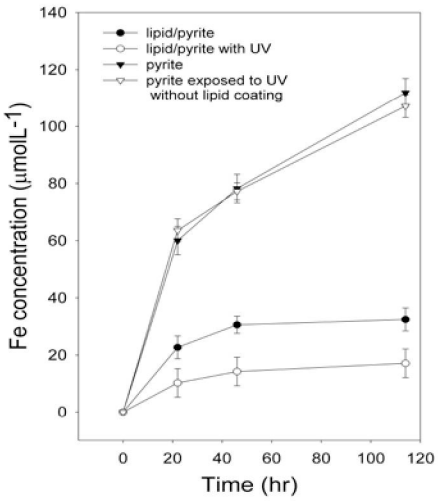

Figure 9: The amount of iron release (i.e., pyrite oxidation) for a given time interval is lowest for the lipid/pyrite surface that had been exposed to UV radiation prior to the start of the Fe release measurements.

In general, experimental observations suggest that the lipids, which contain 2 hydrophobic tails per head group, are at least in part bilayer structures. It is hypothesized that these adsorbed structures provide a hydrophobic pocket that inhibits the interaction

of water and dissolved oxygen with the pyrite surface. In essence, the lipid interrupts the advection of aqueous oxidants or the electron transfer between oxidants and the pyrite.

Surface reactivity of Pyrite in the biotic environment

A) ***Suppression of pyrite oxidation under biotic conditions***

Studies also investigated the effect of bacteria on the oxidation of metal-sulfides, primarily pyrite. Prior research from our laboratory has shown that the adsorption of two-tail lipids of phosphocholine lipids, such as L-α-Phosphatidylcholine, Hydrogenated (Egg, Chicken) lipid and 1,2-bis(10,12-tricosadiynoyl)-*sn*-Glycero-3-Phosphocholine on pyrite resulted in a marked decrease in oxidation rate. We showed that the application of these phospholipids to pyrite surfaces prior to exposure to bacteria led to a significant reduction in the oxidation of the mineral. We initiated research to investigate the behavior of these organic overlayers when they come in contact with pyrite that has been already exposed to bacteria. One might speculate this is a scenario closer to the natural AMD case where bacteria is naturally exposed to bacteria (i.e., *Acidithiobacillus ferrooxidans)*. Hence, any remediation method needs to work in such a system.

Figure 2 exhibits pyrite oxidation data showing that if the bacteria *Acidithiobacillus ferrooxidans* (common to AMD environments) is in contact with pyrite, the oxidation is greatly accelerated relative to abiotic conditions (compare A.F./pyrite to pyrite data in Figure 7). If lipid is first adsorbed on the pyrite surface the oxidation is reduced greatly, resulting in a rate reduction of over a factor of 5.

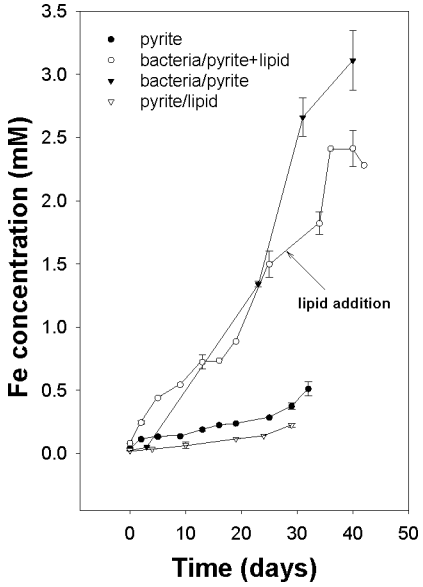

Figure 10: The addition of lipid to pyrite already exposed to bacteria results in a reduction in the mineral oxidation rate. AFM results shown next suggest that lipid displaces bacteria from pyrite.

We also investigated the effect of phospholipids on pyrite surfaces that have been pre-exposed to bacteria (i.e., *Acidithiobacillus ferrooxidans*). Figure 8 exhibits a series of AFM micrographs that show a bacteria laden pyrite surface before and after the introduction of phospholipid. To carry out this particular experiment, an acid washed pyrite platelet was exposed to a bacteria-containing solution for 4 days. The sample was removed (moisture was not removed) from the solution and immediately transferred in to an AFM flow cell where a pH 2 bacteria-sustaining growth solution was flowed over the sample. Image 3a was acquired 0.5 h after the introduction of the sample into the AFM flow cell. The image shows the presence of features ranging from 200 - 600 nm high that we contend are bacteria bound to the pyrite surface (enclosed by white ovals and square). We also make a distinction to the type of bacterial binding and suggest that the higher features are associated with bacterial micro-colonies (bounded by white ovals on Figure 3) on the pyrite. The remaining features with heights

near 200 nm are proposed to be associated with individual bacteria (bounded by white squares). The presence of micro-colonies and individually bound bacteria on the pyrite surface is consistent with prior ex situ work from our laboratory that used epifluorescence microscopy to characterize bacterial growth on pyrite powder. We emphasize that repeated scanning of this area with AFM resulted in no noticeable change in the bacterial surface population. Image 3b was obtained 10 minutes after introduction of phospholipid, and except for some drift of the scanning zone, a fraction of the bacteria was removed from the surface (e.g., compare area 1 bounded by the oval ring in 3a and 3b). We note that a phospholipid concentration was used that was a factor of 4 less than that used in prior studies, due to the difficulty of in situ imaging in solutions with high phospholipid contributions. We attribute the change in the micrograph to the rapid phospholipid-induced displacement of bacteria attached to pyrite. Image c was obtained 30 minutes after the introduction of phospholipid-bearing solution at a pH of 2. Inspection of the image shows that there is a still further loss of bacteria from area 1 and that there is a loss of bacteria that initially were located in area 2. For the rather short times used in our in situ experiments (1 h exposure), we generally experimentally observe little displacement of individually bound bacteria (see area 3, white squares) from the pyrite surface. The experiments presented here suggest that the majority of the bacteria that are displaced from the surface were initially bound in micro-colonies. Image 3d was obtained 1 h after image 3c and is essentially the same as the image acquired 0.5 h after phospholipid introduction (spectrum c). Our interpretation of these AFM images is that the introduction of phospholipid resulted in the loss of a fraction of the surface-bound bacteria, and this conclusion is consistent with our ex situ ATR-FTIR measurements presented above. The impact of this finding on a possible remediation strategy is currently being investigated.

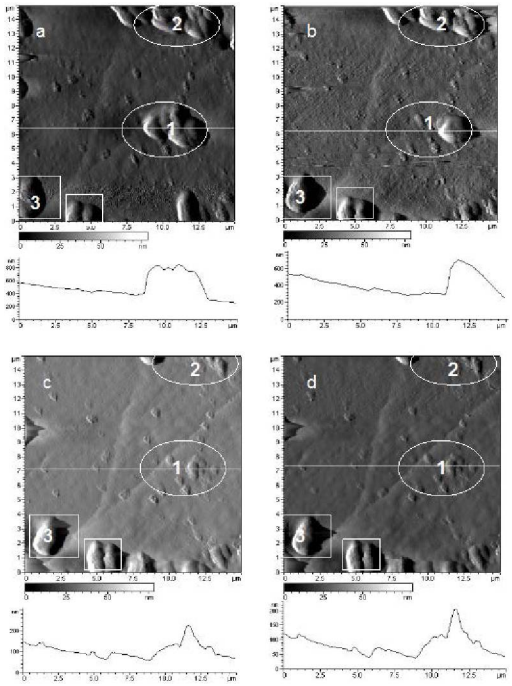

Figure 8: AFM images showing (a) pyrite with bound bacteria, (b) 10 min after lipid introduction, (c) 0.5 h after lipid, and (d) 1.6 h after lipid was added to the solution.

Publications Resulting from Grant DEFG029ER14644

PART I

1. Martin A. A. Schoonen, Elizabeth C. Sklute, M. Darby Dyar et al., "Reactivity of sandstones under conditions relevant to geosequestration: 1. Hematite-bearing

sandstone exposed to supercritical carbon dioxide commingled with aqueous sulfite or sulfide solutions," Chemical Geology **296-297**, 96-102 (2012)
2. Riley Murphy, Kristin Lammers, Alexander Smirnov et al., "Hematite reactivity with supercritical CO2 and aqueous sulfide," Chemical Geology **283** (3-4), 210-217 (2011)
3. Kristin Lammers, Riley Murphy, Amber Riendeau et al., "CO2 Sequestration through Mineral Carbonation of Iron Oxyhydroxides," Environmental Science & Technology **45** (24), 10422-10428 (2011)
4. Daniel R. Strongin, Clare P. Grey, John B. Parise et al., "Surface science studies of environmentally relevant iron (oxy)hydroxides ranging from the nano to the macro-regime," Surface Science **604** (13-14), 1065-1071 (2010)
5. Martin A. A. Schoonen, Andrea D. Harrington, Richard Laffers et al., "Role of hydrogen peroxide and hydroxyl radical in pyrite oxidation by molecular oxygen," Geochimica et Cosmochimica Acta **74** (17), 4971-4987 (2010)
6. Riley Murphy, Kristin Lammers, Alexander Smirnov et al., "Ferrihydrite phase transformation in the presence of aqueous sulfide and supercritical CO2," Chemical Geology **271** (1-2), 26-30 (2010)

PART II

7. Riley Murphy and Daniel R. Strongin, "Surface reactivity of pyrite and related sulfides," Surface Science Reports **64** (1), 1-45 (2009)
8. Jun Hao, Riley Murphy, Eelin Lim et al., "Effects of phospholipid on pyrite oxidation in the presence of autotrophic and heterotrophic bacteria," Geochimica et Cosmochimica Acta **73** (14), 4111-4123 (2009)
9. Alexander Smirnov, Douglas Hausner, Richard Laffers et al., "Abiotic ammonium formation in the presence of Ni-Fe metals and alloys and its implications for the Hadean nitrogen cycle," Geochemical Transactions **9**, No pp given (2008)
10. Xiang V. Zhang, Treavor A. Kendall, Jun Hao et al., "Physical Structures of Lipid Layers on Pyrite," Environmental Science and Technology **40** (5), 1511-1515 (2006)
11. Jun Hao, Curtis Cleveland, Eelin Lim et al., "The effect of adsorbed lipid on pyrite oxidation under biotic conditions," Geochemical Transactions **7**, 1-9 (2006)
12. Corey A. Cohn, Steffen Mueller, Eckard Wimmer et al., "Pyrite-induced hydroxyl radical formation and its effect on nucleic acids," Geochemical Transactions **7**, 1-11 (2006)
13. Courtney R. Usher, Kristian W. Paul, Jayakumar Narayansamy et al., "Mechanistic Aspects of Pyrite Oxidation in an Oxidizing Gaseous Environment: An in Situ HATR-IR Isotope Study," Environmental Science and Technology **39** (19), 7576-7584 (2005)
14. Martin A. Schoonen and Daniel R. Strongin, "Catalysis of electron transfer reactions at mineral surfaces," Environmental Catalysis, 37-60 (2005)
15. Corey A. Cohn, Aimee Pak, Daniel Strongin et al., "Quantifying hydrogen peroxide in iron-containing solutions using leuco crystal violet," Geochemical Transactions **6** (3), 47-51 (2005)

16. Courtney R. Usher, Curtis A. Cleveland, Jr., Daniel R. Strongin et al., "Origin of Oxygen in Sulfate during Pyrite Oxidation with Water and Dissolved Oxygen: An In Situ Horizontal Attenuated Total Reflectance Infrared Spectroscopy Isotope Study," Environmental Science and Technology **38** (21), 5604-5606 (2004)
17. Michael J. Borda, Daniel R. Strongin, and Martin A. Schoonen, "A vibrational spectroscopic study of the oxidation of pyrite by molecular oxygen," Geochimica et Cosmochimica Acta **68** (8), 1807-1813 (2004)
18. Xiang Zhang, Michael J. Borda, Martin A. A. Schoonen et al., "Pyrite oxidation inhibition by a cross-linked lipid coating," Geochemical Transactions, 8-11 (2003)
19. Xiang Zhang, Michael J. Borda, Martin A. A. Schoonen et al., "Adsorption of Phospholipids on Pyrite and Their Effect on Surface Oxidation," Langmuir **19** (21), 8787-8792 (2003)
20. Alicia R. Elsetinow, Daniel R. Strongin, Michael J. Borda et al., "Characterization of the structure and the surface reactivity of a marcasite thin film," Geochimica et Cosmochimica Acta **67** (5), 807-812 (2003)
21. Alicia R. Elsetinow, Michael J. Borda, Martin A. A. Schoonen et al., "Suppression of pyrite oxidation in acidic aqueous environments using lipids having two hydrophobic tails," Advances in Environmental Research **7** (4), 969-974 (2003)
22. Michael J. Borda, Daniel R. Strongin, and Martin A. Schoonen, "A novel vertical attenuated total reflectance photochemical flow-through reaction cell for Fourier transform infrared spectroscopy," Spectrochimica Acta, Part A: Molecular and Biomolecular Spectroscopy **59A** (5), 1103-1106 (2003)
23. Michael J. Borda, Daniel R. Strongin, and Martin A. Schoonen, "A vibrational spectroscopic study of the oxidation of pyrite by ferric iron," American Mineralogist **88** (8-9), 1318-1323 (2003)
24. Michael J. Borda, Alicia R. Elsetinow, Daniel R. Strongin et al., "A mechanism for the production of hydroxyl radical at surface defect sites on pyrite," Geochimica et Cosmochimica Acta **67** (5), 935-939 (2003)